ACS APPLIED NANO MATERIALS

Article

Cite This: ACS Appl. Nano Mater. 2020, 3, 789−796

www.acsanm.org

Dragonfly-Wing-Inspired Inclined Irregular Conical Structures for Broadband Omnidirectional Antireflection Coatings

Chen-Yu Chien, Yu-Han Chen, Ru-Yu Chen, and Hongta Yang*

Department of Chemical Engineering, National Chung Hsing University, 145 Xingda Road, Taichung 40227, Taiwan

Supporting Information

ABSTRACT: Blue-tailed forest hawk dragonfly (*Orthetrum triangulare*) wings exhibit a high transparency at wide viewing angles. The broadband omnidirectional antireflection behaviors of dragonfly wings result from the random arrangement of inclined irregular conical structures. In this study, a scalable colloidal lithography technique is developed for spin-coating randomly packed silica colloids, which serve as direct structural templates for patterning subwavelength inclined conical structures on substrates. The dragonfly-wing-inspired structures feature an omnidirectional antireflection performance over the whole visible spectral range and generate superhydrophobicity after surface functionalization. The dependencies of the inclination and height of the conical structures on the antireflection performance and self-cleaning property are also systemically studied in this research.

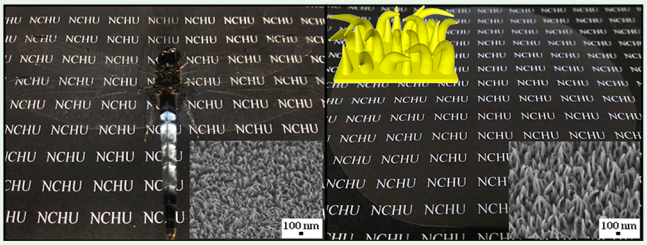

KEYWORDS: *blue-tailed forest hawk dragonfly wing, broadband omnidirectional antireflection, inclined conical structures, colloidal lithography, superhydrophobicity*

INTRODUCTION

Over the past decade, numerous inorganic optical components have been replaced by polymer optics due to the polymer materials possessing a high mechanical stability, high optical transmission, low density, fast processability, and high degree of design freedom, which significantly improve the manufacturability with satisfactory precision.[1] As a result, optical-grade polymers have been extensively exploited for various sophisticated optical, optoelectronic, and photovoltaic devices, as well as electro-optical applications, such as display screens, optical lens, photodetectors, and disposable medical optics.[2] Even though most polymers are highly transparent, excess reflection at the polymer surface degrades the optical performance and incurs serious damage to image legibility.[3] The light reflection, also known as Fresnel reflection, takes place as light impinges at the interface of different media owing to the refractive index change.[4] To address these issues, single-layer antireflection coatings and porous antireflection coatings are extensively employed to minimize surface reflection.[5] The coatings render the destructive interference of light at the media interface to reduce the reflected light intensity. Unfortunately, this methodology suffers from a limited choice of low refractive index coating materials, and the antireflection characteristics of the coatings are narrowband and only for a small incidence angle range.[6]

To effectively depress Fresnel reflection, eliminating the abrupt change of refractive index by engineering structures with a graded refractive index transition on material surfaces provides a different strategy. Generally, multilayer antireflection coatings and antireflective structures are adopted to change the refractive index gradually from air to materials along the normal direction.[7,8] In contrast with single-layer and porous antireflection coatings, multilayer antireflection coatings exhibit broadband antireflection behaviors; however, with complexity comes further more manufacturing and design challenges.[9] Additionally, such coatings are subjected to an incident angle-dependent antireflection characteristic, where the reflected light intensity is enhanced with increasing incident angle. An alternative to the multilayer antireflection coatings is the introduction of antireflective structured surfaces.

Nature has provided diversified strategies through years of evolution to solve varied and versatile survival challenges that largely go unseen, for example, camouflage by transparent cicada wings, requiring high transparency as well as minimalized light scattering.[10] The cicadas take advantage of the antireflective structures found on their wings to surmount the dazzling generated during flying.[11] It is well-known that the hexagonal arrays of non-close-packed subwavelength conical structures on antireflective cicada wings make tracking by predatory birds troublesome.[12] Indeed, similar sized and hexagonally packed conical structures are found on glasswing butterfly wings, hawk moth wings, and moth eyes to create a refractive index gradient for inhibiting Fresnel reflection at normal incidence.[13] Interestingly, the arrangements and structures found on the wing membranes of specific dragonflies, such as the blue-tailed forest hawk dragonfly (*Orthetrum triangulare*), are far from being regular.[14] The irregular positioning and randomly sized conical structures are

Received: November 23, 2019
Accepted: December 19, 2019
Published: December 19, 2019

DOI: 10.1021/acsanm.9b02301
ACS Appl. Nano Mater. 2020, 3, 789−796

the origin of a remarkable broadband antireflection property at a wide angle of incidence.[15] As is well-known, these wings are covered with an epicuticular wax film to achieve prominent hydrophobicity and restrain the penetration of water.[16] The special structures, cooperating with hydrophobic materials, lead to the realization of superhydrophobicity and a self-cleaning functionality.

Inspired by the multifunctional bioarchetypes, researchers have developed a vast range of technologies that can be extensively applied to fabricate biomimetic antireflective structured surfaces for both fundamental research and practical applications.[17] However, most current lithography-based technologies, including ion beam lithography, optical lithography, scanning probe lithography, and nanoimprint lithography, for generating structured surfaces are restricted by time consumption and expense owing to the tedious serial processing, as well as the low resolution of small features caused by surface damage and contamination.[18] Recently, metals have been deposited on silicon substrates by e-beam evaporation, followed by a thermal annealing process, to create irregularly shaped and sized metal islands.[19,20] The metal islands then serve as etching masks during a dry etching procedure to develop subwavelength antireflective structures. Although broadband antireflection at a wide angle of incidence can be achieved, the approaches suffer from complex and costly fabrication procedures. In addition, the high annealing temperature cannot be applied to polymer substrates.

In contrast, colloidal lithography has been widely explored as a simple and inexpensive alternative to conventional lithographic techniques for the fabrication of antireflective structures.[21] A monolayer of colloidal particles is deposited on the material surface and functions as a structural template during a reactive ion etching procedure for patterning the structures.[22] Unfortunately, most of the available deposition technologies for creating colloidal templates, including the Langmuir−Blodgett technique, gravitational sedimentation, convective assembly, and the dip-coating technique, are afflicted with a low throughput and are incompatible with standard microfabrication routines. Due to their thermodynamic stability, only hexagonally close-packed crystal structures are accessible through the above deposition technologies, whereas a non-close-packed arrangement of colloids is favored for creating biomimetic structures. Fueled by the rapid development of surface patterning techniques, numerous post-treatments, such as dry etching and wet etching, have been applied to close-packed colloidal crystals to make non-close-packed arrangements.[23,24] The non-close-packed colloids can then be applied as a structural template to develop antireflective structures. However, it is still a challenge to have colloidal masks retain their original symmetrical shapes during size reduction.[25] Moreover, the antireflection characteristics of most reported subwavelength structures are observed only for incidence angles close to normal incidence.

Recently, a microfabrication-compatible shear force-induced self-assembly technology, developed by Jiang et al., has been used to resolve the aforementional technical obstacles of colloidal technologies.[26,27] This single-step assembly technology enables the creation of non-close-packed colloidal silica crystals on silicon substrates. The silica colloids can then function as an etching mask in a dry etching process to sculpt structure arrays on the silicon surface, which can serve as a second-generation template to replicate antireflective structures on polymers.[28] Nevertheless, this multistep soft-lithography-like replication exhibits a difficulty with high-resolution registration.[29,30]

Owing to their remarkable broadband omnidirectional antireflection properties, blue-tailed forest hawk dragonfly wings are investigated as a prototype in this research. Meanwhile, this work develops a simple and scalable method via modifying the previously mentioned spin-coating technology to directly and randomly deposit non-close-packed colloids on polyethylene terephthalate (PET) substrates, which have been extensively used for optical applications. The colloids then serve as a structural template to pattern dragonfly-wing-like inclined conical structures, which are irregularly arranged and feature a random height. Additionally, the structured PET film is surface functionalized to further improve the surface hydrophobicity. This study systematically characterizes the antireflection performance and self-cleaning functionality of the bioinspired antireflective structures to engineer broadband omnidirectional antireflection coatings for practical applications.

EXPERIMENTAL METHODS

Reagents and Substrates. The chemicals and solvents applied for synthesizing spherical silica colloids, including tetraethyl orthosilicate (TEOS) (98 vol %), aqueous ammonium hydroxide (28 vol %), and anhydrous ethanol (200 proof), were purchased from Sigma-Aldrich. Ultrapure water obtained from a Milli-Q Advantage A-10 water purification system presents a resistivity of 17.9 MΩ·cm at 25 °C and is used directly in all experiments. The UV-curable monomer, ethoxylated trimethylolpropane triacrylate (ETPTA) (SR 454), and the photoinitiator, 2-hydroxy-2-methyl-1-phenyl-1-propanone (Darocur 1173), used in the study were provided by Sartomer Company Corporation and BASF Corporation, respectively. The surface modifier, (tridecafluoro-1,1,2,2,-tetrahydrooctyl)-trichlorosilane (96 vol %), used for surface functionalization was purchased from Thermo Fisher Scientific. PET films with a thickness of approximately 0.01 cm were obtained from Wisegate Technology.

Preparation of Silica Colloidal Suspensions. Monodispersed spherical silica colloids were synthesized according to the Stöber methodology.[31] Typically, aqueous ammonium hydroxide and ultrapure water are mixed with anhydrous ethanol, followed by the rapid injection of TEOS and stirring at 25 °C for 24 h. The as-synthesized silica colloids were purified using anhydrous ethanol by multiple centrifugation and redispersion cycles to remove excess/unreacted chemicals. After the supernatant solvent was discarded, the purified silica colloids were dispersed in the nonvolatile ETPTA monomer with 1 vol % Darocur 1173 by using an ultrasonic homogenizer (Esquire Biotech). The colloid volume fraction of the silica colloidal suspension was controlled to be 25 vol %.

Fabrication of a Monolayer of Randomly Packed Silica/Polymer Composite. After filtration to remove any particle aggregates, the as-prepared silica colloidal suspension was deposited and spread on a PET film, which was cleaned in a mixture of ultrapure water and anhydrous ethanol for 30 min before using. The PET film was spun at 250 rpm for 60 s, 500 rpm for 60 s, 1000 rpm for 30 s, 2500 rpm for 30 s, 5000 rpm for 30 s, and 7000 rpm for 240 s to remove excess suspension using a spin processor (Laurell Technologies, WS-400B-6NPP-Lite). After coating, the ETPTA monomer was photopolymerized via a UV curing system (OPAS, X Lite 500 Pulsed) for 5 s.

Template Fabrication of PET Conical Structures. The as-prepared monolayer silica/polymer composite-coated PET substrates were placed in a Unaxis Shuttlelock RIE/ICP reactive ion etcher, and the chamber pressure was 20 mTorr with a fixed oxygen flow rate of 20 sccm. The embedded silica colloids were released by oxygen reactive ion etching (RIE) for 1 min. The monolayer of silica colloids then serves as a structural template during the second RIE procedure, operating at a 20 mTorr chamber pressure with an oxygen flow rate of

DOI: 10.1021/acsanm.9b02301
ACS Appl. Nano Mater. 2020, 3, 789−796

5 sccm and an argon flow rate of 15 sccm, for directly patterning conical structures on the substrate. The silica structural template could then be wet etched in an ethanol solution containing hydrofluoric acid (2 vol %) for 3 min and rinsed with anhydrous ethanol.

Surface Functionalization of PET Conical Structures. The surface hydrophobicity of the conical-structure-covered PET substrate was improved by being chemically functionalized with fluorosilane through a chemical vapor deposition procedure. In this study, the conical-structure-covered PET substrate was placed in a vacuum oven with an open vial containing (tridecafluoro-1,1,2,2-tetrahydrooctyl)-trichlorosilane. The fluorosilane molecules were vaporized at 60 °C and reacted with the hydroxyl groups on the conical structures.[32,33] After 1.5 h, the PET substrate was transferred to another vacuum oven, which was evacuated to volatilize any unreacted fluorosilane molecules remaining on the conical structures.

Characterization. Photographic images of the specimens were acquired using a Canon digital camera (PowerShot SX740 HS). The surface morphology of the specimens was observed on a field-emission scanning electron microscope (FEG-SEM, JEOL 6335F) after sputtering a platinum layer onto the specimens. Reflection and transmission spectra were obtained by using a high-resolution UV–visible–near-IR spectrometer (Ocean Optics HR4000) with a tungsten–halogen light source and an optic fiber probe (R-400-7-SR) in a wavelength range from 300 to 800 nm. A KRÜSS G10 sessile drop shape analyzer with an imaging system was employed to determine the water contact angle of the specimens. Using an autopipetting system, 5 μL of ultrapure water droplets was dispensed onto the specimens before the images were taken. The procedure was repeated 10 times in different regions of each specimen, and the water contact angle of each image was analyzed and averaged using DropSnake software.

RESULTS AND DISCUSSION

Dragonflies make use of sub-micrometer-scale wax structures on the wing membrane surface to achieve low reflection and to minimize light scattering.[34] For instance, blue-tailed forest hawk dragonfly (*Orthetrum triangulare*) wings feature a low haze and remarkable high transparency, even for large viewing angles of 60° (Figure 1a,b). The omnidirectional antireflection performance originates from the irregular positioning of inclined irregular conical structures covering the transparent dragonfly wings (Figure 1c). As displayed in Figure 1d, the disorderedly arranged conical structures are separated from each other with an average distance of 100 nm. The randomness is limited to not only the conical structure arrangement but also the height of the conical structures. It is found that the structure height varies and presents typical values between 70 and 180 nm, which are less than visible-light wavelengths. Additionally, the histogram of the height ranks is an approximately Gaussian distribution with a variance of approximately 40 nm (Figure S1).

Inspired by the dragonfly wing structures and their role in omnidirectional antireflection, the inclined conical structures are built through a combination of a spin-coating technology and a colloidal lithography process. As displayed in the experimental scheme (Figure 2), a monolayer of a randomly packed silica/polymer composite is spin-coated onto a cleaned PET substrate, followed by an oxygen and argon RIE process. Given the nature of reactive ion etching, a high selectivity between silica and polymer is achieved in the RIE treatments, with the silica colloids functioning as a structural template and preserving the polymer substrate underneath, resulting in the configuration of mushroom-like features.[35] The sizes and aspect ratios of the polymer stems are easily controlled by adjusting the RIE conditions and the silica cap size. Interestingly, the polymer stem tips are too thin to support the above silica caps after a long RIE duration, leading to the formation of inclined enoki-mushroom-like features. The silica caps of the inclined enoki-mushroom-like features are then wet etched to pattern the dragonfly-wing-inspired inclined conical structures directly on the PET substrate.

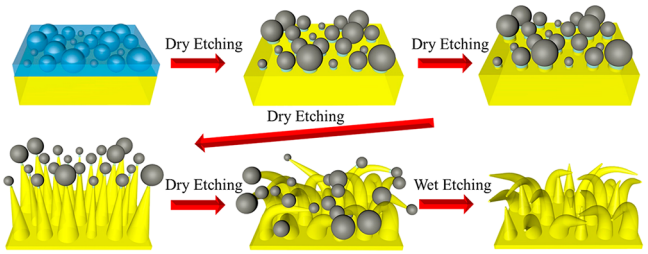

Figure 2. Schematic illustration of the experimental procedures for fabricating the dragonfly-wing-inspired antireflection coating.

To biomimic the randomly arranged inclined conical structures with Gaussian-distributed sizes on dragonfly wings, a silica colloidal suspension consisting of 70 nm silica colloids, 130 nm silica colloids, and 180 nm silica colloids is spin-coated on a PET substrate, followed by a UV polymerization process. The amounts of 70, 130, and 180 nm silica colloids follow a ratio of 1:2:1. As displayed in Figure 3, a monolayer of 70 nm silica/130 nm silica/180 nm silica/polymer composite is

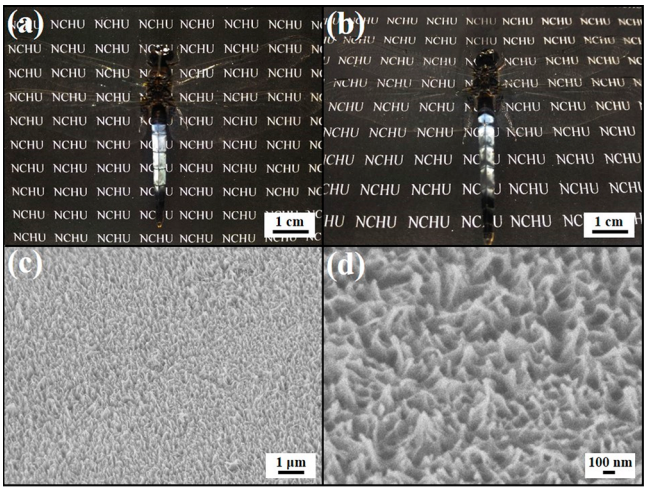

Figure 1. Photographic images of a dragonfly (*Orthetrum triangulare*) taken from (a) 0° and (b) 60°. (c) Side-view SEM image of the dragonfly wing in (a). (d) Magnified SEM image of (c).

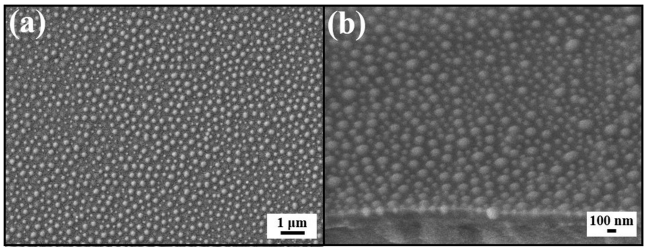

Figure 3. (a) Top-view SEM image of a 70 nm silica/130 nm silica/180 nm silica/polymer composite. (b) Magnified side-view SEM image of (a).

DOI: 10.1021/acsanm.9b02301
ACS Appl. Nano Mater. 2020, 3, 789–796

coated on the PET substrate. Although a few aggregated silica colloids are observed, it is evident that most silica colloids are apart from each other and with an average spacing of approximately 100 nm.

The polymer part of the silica/polymer composite coated on the PET substrate is then selectively plasma etched by concurrent oxygen and argon reactive ions for 5, 7.5, 10, or 12.5 min, and the randomly arranged silica colloids protect the PET substrate underneath. Importantly, the introduction of isotropic oxygen plasma etching and anisotropic argon plasma etching results in the formation of enoki-mushroom-like features consisting of mushroom-cap-like silica tops and mushroom-stem-like polymer bottoms (Figure 4). The top

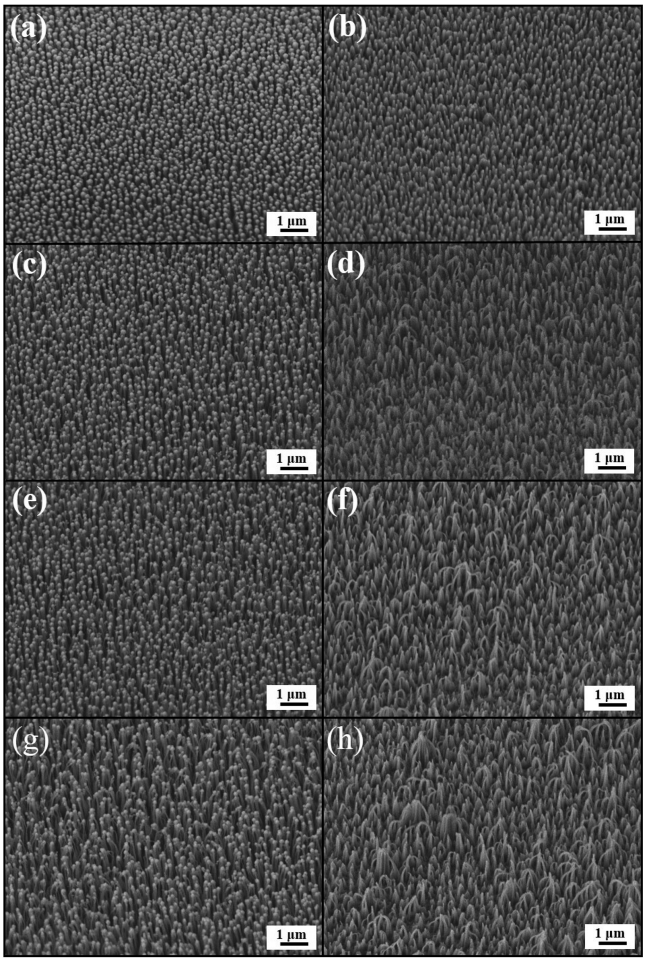

Figure 4. Side-view SEM images of enoki-mushroom-like structures and the corresponding PET conical structures obtained with different RIE durations: (a,b) 5 min; (c,d) 7.5 min; (e,f) 10 min; (g,h) 12.5 min.

silica spherical structures can finally be wet etched to create randomly arranged conical structures directly on the PET substrate. It is evident that the residual PET conical structures are well retained and separated from each other. In addition, the randomness is limited to not only the conical structure arrangement but also the size distribution. Although the size of the silica tops does not shrink significantly under the RIE treatment, a longer RIE treatment results in the constitution of sharper and taller conical structures (Figure S2). Interestingly, as the RIE duration reaches 7.5 min, the PET conical structures are sharpened to the point that the tops sufficiently cannot support the above silica spherical structures sufficiently, leading to inclined conical structures (Figure 4d). Figure S2b and the magnified SEM images in Figure S3a,b reveal that the heights of the inclined conical structures range from 100 to 200 nm, and the average interstructural spacing is approximately 100 nm. The surface morphology of the as-prepared coating is very similar to the inclined irregular conical structures found on the transparent dragonfly wings (Figure S3c,d). It is worth mentioning that the randomly arranged non-close-packed silica templates provide ample space for the formation of inclined conical structures. For the RIE duration of 10 min, the shaped conical structures are not capable of supporting the above silica spherical structures, resulting in serious inclination. As displayed in Figure 4f, although the conical structures are maintained, seriously inclined conical structures are bunched, mainly in groups of two between neighboring conical structures, after removing the silica spherical structures. The random bunching is attributed to the van der Waals forces among adjacent structures with high aspect ratios attributed to randomly bunching.[36−38] With the further increase in the RIE treatment to 12.5 min, the bunching is further exasperated, and several inclined conical structures are bunched into conical shape aggregates (Figure 4h).

As presented previously, periodic conical structures with high aspect ratios are capable of efficiently reducing optical reflection from normal incidence by creating a refractive index gradient near the air/substrate interface, biomimicking the antireflective principle of cicada wings.[39] To analyze antireflection capability of the dragonfly-wing-inspired conical structures displayed in Figure 4, the optical reflection spectra of a bare PET substrate (black curve) and five templated conical-structure-covered PET substrates prepared by different RIE durations (0, 5, 7.5, 10, and 12.5 min) are evaluated at normal incidence (Figure 5). The featureless PET film exhibits

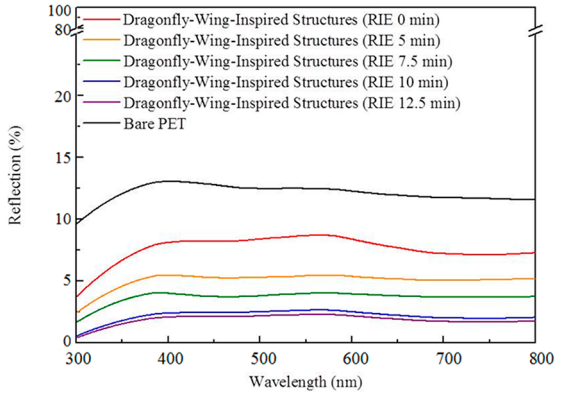

Figure 5. Normal incidence optical reflection spectra obtained from a bare PET substrate and PET substrates coated with PET conical structures acquired from different RIE durations.

a high reflection (>10%) in the visible wavelength region, conforming with the observations of previous work.[40] Compared with that result, specular reflections are suppressed by the conical structures on the PET substrate. Evidently, a longer RIE treatment results in a lower specular reflection over the whole spectrum, indicating that the broadband antireflection capability of the conical structures can be improved by increasing the RIE duration. It is worth mentioning that the sample with the monolayer silica/polymer composite coated

DOI: 10.1021/acsanm.9b02301
ACS Appl. Nano Mater. 2020, 3, 789−796

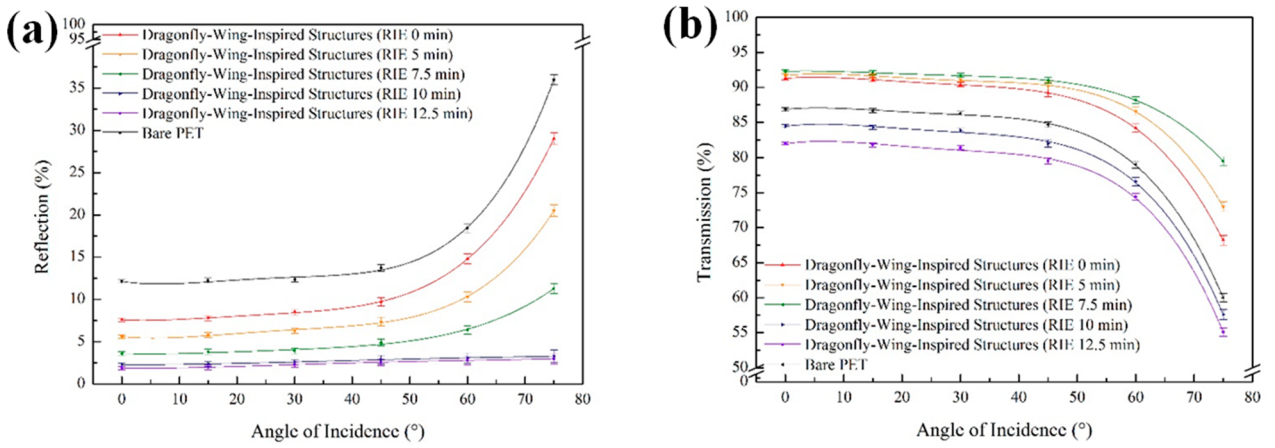

Figure 6. (a) Optical reflection spectra and (b) optical transmission spectra at various incidence angles obtained from a bare PET substrate and PET substrates coated with PET conical structures acquired from different RIE durations.

on the PET substrate (no plasma etching treatment) exhibits an optical reflection lower than that of the featureless PET substrate. The random non-close-packed silica hemispherical structures, as displayed in Figure 3, provide a gradual refractive index transition on the surface and therefore facilitate the suppression of normal incident specular reflection.

To better understand the structure−shape effect on the antireflective property, the average optical reflections and average optical transmissions of the visible-light wavelength region for all the mentioned specimens are evaluated at various incidence angles from 0 to 75°. The results in Figure 6a reveal that the average optical reflections in the visible-wavelength region of both the featureless PET substrate and the conical-structure-covered PET substrates increase with the incidence angles. Additionally, it is evident that the dragonfly-wing-inspired conical structures obtained with a long RIE duration can effectively suppress optical reflection, even for large angles of incidence. Although the reflections of conical-structure-covered substrates achieved with 10 and 12.5 min RIE durations treatments are reduced to less than 2% for wide incidence angles (Figure 6a), the transmissions of those substrates are lower than those of the other etched samples (Figure 6b). Clearly, the antireflection properties are greatly impaired by introducing bunched conical structures (Figure 4f) and micrometer-scale conical shape aggregates (Figure 4h), which are larger than the visible-light wavelengths. The incident visible light is therefore internally reflected and refracted within the structures. Instead, the optical transmission spectra disclose that the transmissions of the conical-structure-covered substrates increase with the RIE duration (0, 5, and 7.5 min) at various incident angles. The specimen prepared by RIE for 7.5 min shows an average transmission over the whole visible spectrum that is approximately 5% higher than that of the featureless specimen at 0° (normal incidence). Importantly, the average transmission is even approximately 22% higher at 75°, which indicates that the broadband omnidirectional antireflection capability can be designed and constructed by introducing inclined irregular conical structures on the polymer surface.

The antireflection performance of the PET substrate coated with conical structures attained with a 7.5 min RIE treatment is further verified through a comparison with that of dragonfly (*Orthetrum triangulare*) wings. As shown in Figure S4, the optical reflection spectra and optical transmission spectra of dragonfly wings show a tendency very similar to that in the spectra of the as-fabricated dragonfly-wing-inspired structure-coated PET substrate. These results suggest that the broadband omnidirectional antireflective property can be increased by biomimicking the inclined conical structures on dragonfly wings. With subwavelength interconical structure distances, an effective medium theory can be employed to explain the incident light propagation at the air/substrate interface.[41] The effective refractive indexes of conical structures obtained with longer RIE durations increase gradually from air to the substrate. The smooth refractive index gradients at various angles exhibited by the randomly inclined conical structures generate low reflection for the visible-light spectrum over a broad range of incidence angles.

Figure 7 displays photographic images of a bare PET substrate (Figure 7a,b) and a PET substrate coated with conical structures achieved with a 7.5 min RIE treatment (Figure 7c,d) illumined by white light. It is observed that the featureless specimen displays a milky color at viewing angles of 0 and 60°, which is caused by the Fresnel reflection of incident light. In contrast, the letters underneath the inclined conical-structure-covered PET substrate are clearly visible, and the

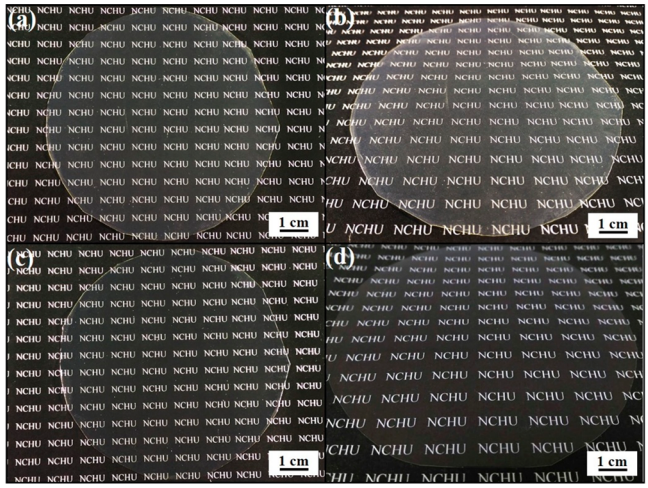

Figure 7. Photographic images of a bare PET substrate taken at (a) 0° and (b) 60°, and a PET substrate coated with PET conical structures obtained after a 7.5 min RIE process taken at (c) 0° and (d) 60°.

DOI: 10.1021/acsanm.9b02301
ACS Appl. Nano Mater. 2020, 3, 789−796

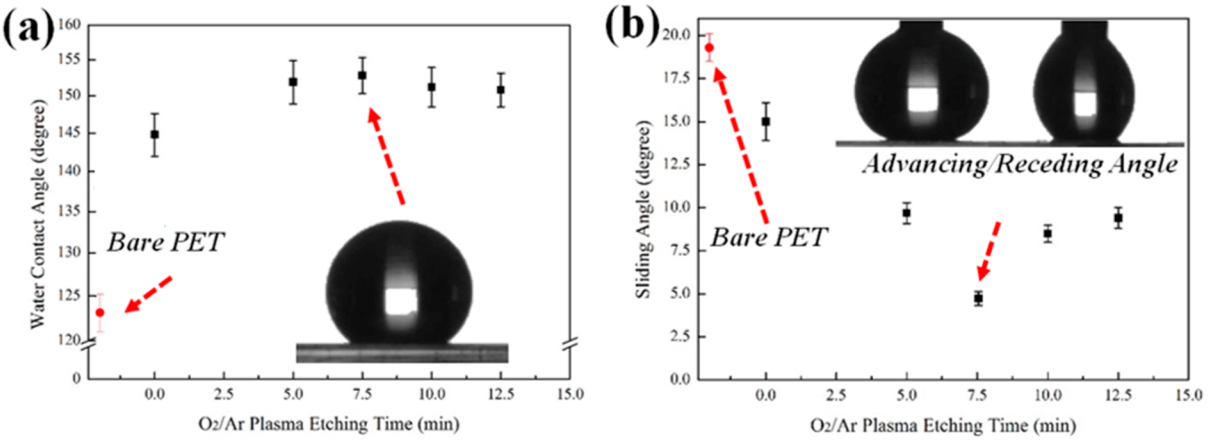

Figure 8. (a) Static water contact angles and (b) sliding angles of PET substrates coated with surface-modified PET conical structures acquired from different RIE durations.

substrate is highly transparent and macroscopically uniform, even for viewing angles up to 60°. The high transparency agrees with the optical behavior of dragonfly wings and further confirms that incident visible light is neither reflected nor scattered off the as-fabricated inclined conical structures. Importantly, in our previous work, periodic conical structure arrays are patterned on polymeric substrates and biomimic transparent cicada wings, which exhibit a high transmittance in the visible region.[42] Even though the templated conical structures exhibit a superior broadband antireflection, the optical transmission decreases with increasing incidence angles, indicating that the antireflection characteristics of the periodic conical structures are only for narrow incidence angles. Compared to that material, the dragonfly-wing-inspired inclined irregular conical structures are randomly arranged and feature a high transmission over the whole visible spectral range for wide viewing angles. The results suggest that large-scale broadband omnidirectional antireflection coatings with a high transparency can be directly patterned on the substrate surface without applying an adhesive layer.

The wax covering irregular conical structures on dragonfly wings renders an exterior hydrophobicity and prevents the penetration of water.[43,44] The conical structures not only reduce optical reflection but also enable superhydrophobic and self-cleaning functionalities. In the study, the as-fabricated dragonfly-wing-inspired antireflective structures are surface modified through a post-treatment with a fluorosilane to improve the surface hydrophobicity. Figure 8a compares the static water contact angles (SWCAs) of the surface-functionalized conical-structure-covered PET substrates with various RIE durations. Apparently, the SWCA of the specimens increases with the RIE duration. The average SWCA on the surface-functionalized featureless PET substrate is 121 ± 2°. By contrast, the water droplet silhouette (inset of Figure 8a) reveals that a superhydrophobic surface with an SWCA of 152 ± 2° can be achieved on a surface-modified PET substrate coated with conical structures from a 7.5 min RIE treatment. For longer RIE treatments, the configuration of micrometer-scale aggregates leads to a slight reduction in the SWCA. This dewetting behavior agrees with the Cassie−Baxter model, which is appropriate for expounding the wetting phenomenon of sub-micrometer-scale structure-covered surfaces.[45] According to the Cassie equation, $\cos\theta' = f\cos\theta - (1 - f)$, the SWCA ($\theta$) on a rough surface can be increased by decreasing the surface area fraction (f) of a hydrophobic material with an intrinsic WCA (θ) larger than 90°. To put it another way, the SWCA increases with the air fraction trapped between the functionalized inclined irregular conical structures, which therefore prevent the substrate from contacting the water droplet.

For most superhydrophobic structured surfaces, water droplets can roll off easily at low tilting angles, and the contaminating particles adhering to the substrate can be picked up and removed by the water droplets. To demonstrate the self-cleaning capability of the surface-functionalized conical-structure-covered substrates, the sliding angles, as well as referring to the difference between advancing and receding contact angles, of the substrates are measured and displayed in Figure 8b. The results disclose that the sliding angle decreases with increasing RIE duration, and a minimum sliding angle of 5° is achieved for the RIE duration of 7.5 min (insets of Figure 8a). It is worth noting that the inclined conical structures exhibit a high surface area fraction in comparison to that of the straight conical structures, leading to larger sliding angles than expected.[46] Furthermore, it is evident that superhydrophobic antireflection coatings with a self-cleaning capability can be implemented on fluorosilane-modified inclined conical-structure-covered substrates.

CONCLUSIONS

To conclude, this research develops a scalable colloidal lithography-based methodology for engineering multifunctional sub-micrometer-scale structures on polymer substrates that biomimic the structures on transparent dragonfly wings. The spin-coated silica colloids, with a random non-close-packed pattern, serve as a structural template to provide adequate space for creating inclined conical structures. The optical analysis reveals that optical reflection is suppressed by introducing inclined irregular conical structures. By optimizing the shape and inclination of the conical structures, broadband antireflective surfaces can be designed and built even for wide viewing angles. The dragonfly-wing-inspired transparent antireflection coating further presents superhydrophobic and self-cleaning properties after surface functionalization and holds promise for various optical applications.

DOI: 10.1021/acsanm.9b02301
ACS Appl. Nano Mater. 2020, 3, 789−796

■ ASSOCIATED CONTENT

Supporting Information

The Supporting Information is available free of charge at https://pubs.acs.org/doi/10.1021/acsanm.9b02301.

Scanning electron microscopy images, statistical analysis of the conical structure height distribution, optical reflection and transmission spectra collected from a dragonfly wing and PET substrates coated with dragonfly-wing-inspired conical structures (PDF)

■ AUTHOR INFORMATION

Corresponding Author

*E-mail: hyang@dragon.nchu.edu.tw.

ORCID

Hongta Yang: 0000-0002-5822-1469

Notes

The authors declare no competing financial interest.

■ ACKNOWLEDGMENTS

This study is supported by the National Science Council under grant numbers MOST107-2221-E-005-035, MOST 108-2221-E-005-040, and MOST 108-2221-E-005-038-MY2.

■ REFERENCES

(1) Li, S.; Liu, Y.; Li, Y.; Liu, S.; Chen, S.; Su, Y. Fast-response Pancharatnam-Berry phase optical elements based on polymer-stabilized liquid crystal. *Opt. Express* **2019**, *27* (16), 22522−22531.

(2) Cao, X.; Lau, C.; Liu, Y.; Wu, F.; Gui, H.; Liu, Q.; Ma, Y.; Wan, H.; Amer, M. R.; Zhou, C. Fully screen-printed, large-area, and flexible active-matrix electrochromic displays using carbon nanotube thin-film transistors. *ACS Nano* **2016**, *10* (11), 9816−9822.

(3) Feng, C.; Gou, T.; Li, J.; Cai, Y.; He, P.; Huang, J.; Wen, Y.; Ma, Y.; Zhang, Z. A highly transparent polymer coating on the glass with broadband antireflection, antifogging and antifouling properties. *Mater. Res. Express* **2019**, *6* (7), 075319.

(4) Dobrowolski, J.; Poitras, D.; Ma, P.; Vakil, H.; Acree, M. Toward perfect antireflection coatings: numerical investigation. *Appl. Opt.* **2002**, *41* (16), 3075−3083.

(5) Berman, D.; Guha, S.; Lee, B.; Elam, J. W.; Darling, S. B.; Shevchenko, E. V. Sequential infiltration synthesis for the design of low refractive index surface coatings with controllable thickness. *ACS Nano* **2017**, *11* (3), 2521−2530.

(6) Choi, K.; Park, S. H.; Song, Y. M.; Lee, Y. T.; Hwangbo, C. K.; Yang, H.; Lee, H. S. Nano-tailoring the surface structure for the monolithic high-performance antireflection polymer film. *Adv. Mater.* **2010**, *22* (33), 3713−3718.

(7) Poitras, D.; Dobrowolski, J. Toward perfect antireflection coatings. 2. Theory. *Appl. Opt.* **2004**, *43* (6), 1286−1295.

(8) Chhajed, S.; Schubert, M. F.; Kim, J. K.; Schubert, E. F. Nanostructured multilayer graded-index antireflection coating for Si solar cells with broadband and omnidirectional characteristics. *Appl. Phys. Lett.* **2008**, *93* (25), 251108.

(9) Zhang, C.; Mcadams, D. A.; Grunlan, J. C. Nano/micro-manufacturing of bioinspired materials: A review of methods to mimic natural structures. *Adv. Mater.* **2016**, *28* (30), 6292−6321.

(10) Meng, Z.; Huang, B.; Wu, S.; Li, L.; Zhang, S. Bio-inspired transparent structural color film and its application in biomimetic camouflage. *Nanoscale* **2019**, *11* (28), 13377−13384.

(11) Han, Z.; Mu, Z.; Li, B.; Niu, S.; Zhang, J.; Ren, L. A High-Transmission, Multiple Antireflective Surface Inspired from Bilayer 3D Ultrafine Hierarchical Structures in Butterfly Wing Scales. *Small* **2016**, *12* (6), 713−720.

(12) Liu, Y.; Song, Y.; Niu, S.; Zhang, Y.; Han, Z.; Ren, L. Integrated super-hydrophobic and antireflective PDMS bio-templated from nano-conical structures of cicada wings. *RSC Adv.* **2016**, *6* (110), 108974−108980.

(13) Shen, L.; Du, H.; Yang, J.; Ma, Z. Optimized broad band and quasi-omnidirectional anti-reflection properties with moth-eye structures by low cost replica molding. *Appl. Surf. Sci.* **2015**, *325*, 100−104.

(14) Song, F.; Xiao, K.; Bai, K.; Bai, Y. Microstructure and nanomechanical properties of the wing membrane of dragonfly. *Mater. Sci. Eng., A* **2007**, *457* (1−2), 254−260.

(15) Siddique, R. H.; Gomard, G.; Hölscher, H. The role of random nanostructures for the omnidirectional anti-reflection properties of the glasswing butterfly. *Nat. Commun.* **2015**, *6*, 6909.

(16) Kurokawa, Y.; Nagai, K.; Huan, P. D.; Shimazaki, K.; Qu, H.; Mori, Y.; Toda, Y.; Kuroha, T.; Hayashi, N.; Aiga, S.; et al. Rice leaf hydrophobicity and gas films are conferred by a wax synthesis gene (LGF 1) and contribute to flood tolerance. *New Phytol.* **2018**, *218* (4), 1558−1569.

(17) Jang, H. J.; Kim, Y. J.; Yoo, Y. J.; Lee, G. J.; Kim, M. S.; Chang, K. S.; Song, Y. M. Double-Sided Anti-Reflection Nanostructures on Optical Convex Lenses for Imaging Applications. *Coatings* **2019**, *9* (6), 404.

(18) Ryu Cho, Y. K.; Rawlings, C. D.; Wolf, H.; Spieser, M.; Bisig, S.; Reidt, S.; Sousa, M.; Khanal, S. R.; Jacobs, T. D.; Knoll, A. W. Sub-10 nm feature size in silicon using thermal scanning probe lithography. *ACS Nano* **2017**, *11* (12), 11890−11897.

(19) Ho, W.-J.; Ou, S.-H.; Lee, Y.-Y.; Liu, J.-J. Broadband wavelength and wide-acceptance angle of the SiO2 sub-wavelength surface structure for solar cells using CF4 reactive ion etching. *Thin Solid Films* **2013**, *529*, 257−262.

(20) Ou, Y.; Aijaz, I.; Jokubavicius, V.; Yakimova, R.; Syväjärvi, M.; Ou, H. Broadband antireflection silicon carbide surface by self-assembled nanopatterned reactive-ion etching. *Opt. Mater. Express* **2013**, *3* (1), 86−94.

(21) Ressier, L.; Viallet, B.; Beduer, A.; Fabre, D.; Fabie, L.; Palleau, E.; Dague, E. Combining convective/capillary deposition and AFM oxidation lithography for close-packed directed assembly of colloids. *Langmuir* **2008**, *24* (23), 13254−13257.

(22) Park, J. Y.; Advincula, R. C. Nanostructuring polymers, colloids, and nanomaterials at the air-water interface through Langmuir and Langmuir-Blodgett techniques. *Soft Matter* **2011**, *7* (21), 9829−9843.

(23) Chen, H.; Chuang, S.; Lin, C.-H.; Lin, Y. Using colloidal lithography to fabricate and optimize sub-wavelength pyramidal and honeycomb structures in solar cells. *Opt. Express* **2007**, *15* (22), 14793−14803.

(24) Ye, X.; Huang, J.; Geng, F.; Liu, H.; Sun, L.; Yan, L.; Jiang, X.; Wu, W.; Zheng, W. High power laser antireflection subwavelength grating on fused silica by colloidal lithography. *J. Phys. D: Appl. Phys.* **2016**, *49* (26), 265104.

(25) Chao, Y.-C.; Wang, K.-R.; Meng, H.-F.; Zan, H.-W.; Hsu, Y.-H. Large-area non-close-packed nanosphere deposition by blade coating for vertical space-charge-limited transistor. *Org. Electron.* **2012**, *13* (12), 3177−3182.

(26) Min, W. L.; Jiang, B.; Jiang, P. Bioinspired self-cleaning antireflection coatings. *Adv. Mater.* **2008**, *20* (20), 3914−3918.

(27) Zhang, C.; Liu, B.; Tang, C.; Liu, J.; Qu, X.; Li, J.; Yang, Z. Large scale synthesis of Janus submicron sized colloids by wet etching anisotropic ones. *Chem. Commun.* **2010**, *46* (25), 4610−4612.

(28) Cho, Y.-S.; Yi, G.-R.; Moon, J. H.; Kim, D.-C.; Lee, B.-J.; Yang, S.-M. Dry etching of colloidal crystal films. *J. Colloid Interface Sci.* **2010**, *341* (2), 209−214.

(29) Jiang, Y.; Shen, H.; Yang, W.; Zheng, C.; Tang, Q.; Yao, H.; Raza, A.; Li, Y.; Huang, C. Passivation properties of alumina for multicrystalline silicon nanostructure prepared by spin-coating method. *Appl. Phys. A: Mater. Sci. Process.* **2018**, *124* (2), 95.

(30) Askar, K.; Phillips, B. M.; Fang, Y.; Choi, B.; Gozubenli, N.; Jiang, P.; Jiang, B. Self-assembled self-cleaning broadband anti-reflection coatings. *Colloids Surf., A* **2013**, *439*, 84−100.

DOI: 10.1021/acsanm.9b02301
ACS Appl. Nano Mater. 2020, 3, 789−796

(31) Stöber, W.; Fink, A.; Bohn, E. Controlled growth of monodisperse silica spheres in the micron size range. *J. Colloid Interface Sci.* **1968**, *26* (1), 62−69.
(32) Cai, C.-Y.; Lin, K.-Y. A.; Yang, H. Superhydrophobic anti-ultraviolet films by doctor blade coating. *Appl. Phys. Lett.* **2014**, *105* (20), 201913.
(33) Yang, H.; Jiang, P. Self-cleaning diffractive macroporous films by doctor blade coating. *Langmuir* **2010**, *26* (15), 12598−12604.
(34) Hooper, I. R.; Vukusic, P.; Wootton, R. Detailed optical study of the transparent wing membranes of the dragonfly Aeshna cyanea. *Opt. Express* **2006**, *14* (11), 4891−4897.
(35) Junkar, I.; Modic, M.; Mozeti, M. Modification of PET surface properties using extremely non-equilibrium oxygen plasma. *Open Chemistry* **2014**, *13* (1), 490−496.
(36) Dev, A.; Chaudhuri, S. Uniform large-scale growth of micropatterned arrays of ZnO nanowires synthesized by a surfactant assisted approach. *Nanotechnology* **2007**, *18* (17), 175607.
(37) Liu, H.; Li, S.; Zhai, J.; Li, H.; Zheng, Q.; Jiang, L.; Zhu, D. Self-Assembly of Large-Scale Micropatterns on Aligned Carbon Nanotube Films. *Angew. Chem., Int. Ed.* **2004**, *43* (9), 1146−1149.
(38) Wei, Z.; Schneider, T. M.; Kim, J.; Kim, H.-Y.; Aizenberg, J.; Mahadevan, L. Elastocapillary coalescence of plates and pillars. *Proc. R. Soc. London, Ser. A* **2015**, *471* (2175), 20140593.
(39) Boden, S. A.; Bagnall, D. M. Tunable reflection minima of nanostructured antireflective surfaces. *Appl. Phys. Lett.* **2008**, *93* (13), 133108.
(40) Lin, C.-Y.; Lin, K.-Y. A.; Yang, T.-W.; Chen, Y.-C.; Yang, H. Self-assembled hemispherical nanowell arrays for superhydrophobic antireflection coatings. *J. Colloid Interface Sci.* **2017**, *490*, 174−180.
(41) Huang, J.; Wang, X.; Wang, Z. L. Bio-inspired fabrication of antireflection nanostructures by replicating fly eyes. *Nanotechnology* **2008**, *19* (2), 025602.
(42) Chen, Y.-C.; Huang, Z.-S.; Yang, H. Cicada-wing-inspired self-cleaning antireflection coatings on polymer substrates. *ACS Appl. Mater. Interfaces* **2015**, *7* (45), 25495−25505.
(43) Gao, C. Y.; Meng, G. X.; Li, X.; Wu, M.; Liu, Y.; Li, X. Y.; Zhao, X.; Lee, I.; Feng, X. Wettability of dragonfly wings: the structure detection and theoretical modeling. *Surf. Interface Anal.* **2013**, *45* (2), 650−655.
(44) Wan, Y.-l.; Cong, Q.; Wang, X.-j.; Yan, Z. The wettability and mechanism of geometric non-smooth structure of dragonfly wing surface. *J. Bionic Eng.* **2008**, *5* (1), 40−45.
(45) Cassie, A.; Baxter, S. Wettability of porous surfaces. *Trans. Faraday Soc.* **1944**, *40*, 546−551.
(46) Ding, W.; Fernandino, M.; Dorao, C. Conical micro-structures as a route for achieving super-repellency in surfaces with intrinsic hydrophobic properties. *Appl. Phys. Lett.* **2019**, *115* (5), 053703.

DOI: 10.1021/acsanm.9b02301
ACS Appl. Nano Mater. 2020, 3, 789−796